

1 **Supplementary Note 1. Conventional 2D grating equation**

2 Eq. 1 governs the angular locations of the principal intensity maxima when light of wavelength λ
3 is diffracted from a horizontal grating of groove spacing d_h (Supplementary Fig. 7a). The grating
4 equation reveals that only the spectral orders for which $|m_h \lambda_h / d_h| < 2$ can exist and hence
5 determines the specific number of allowed modes for the flat grating. However, due to the
6 complex geometry of the prism and foil gratings (i.e. the superposition of microscopic shape
7 and vertical surface nanogratings), the diffraction profiles are rather complex as shown in Fig.
8 6h&i. The diffraction profile by the microscopic horizontal grating also follows Eq. 1 and it allows
9 up to 47 orders for $d = 10 \mu\text{m}$ in the same optical region (Supplementary Fig. 7b).

10 **Supplementary Note 2. Dispersion in the context of diffraction grating**

11 Under a very specific context when discussing diffraction gratings, the term dispersion can be
12 defined as “a measurement of the separation (either angular or spatial) between diffracted light
13 of different wavelengths” according to the DIFFRACTION GRATING HANDBOOK¹. Which can
14 be further separated into angular dispersion – the spectral range per unit angle; and linear
15 dispersion – the spectral range per unit length. Not to be confused with another, and maybe
16 more familiar type of dispersion, the chromatic dispersion, which is defined as the separation of

17 light due to varies wavelength dependent refractive indices of a material, such as the
18 continuous rainbow spectrum produced by a prism.

19 **Supplementary Note 3. Nano-grating/micro-geometry interaction**

20 In order to decouple the effects of microscopic shape versus the surface nanograting of the foil
21 Foil grating structure, we analysed their respective contribution with FEM simulation of overall
22 geometry with (Fig. 4c) and without (Fig. 4d) the surface nanogratings. The foil-shaped
23 structure without surface nanogratings (i.e. a lenticular prism) results in straight lines in the
24 simulated scattering spectra (Supplementary Fig. 6b) caused by the horizontal periodicity of a
25 unit cell, and such observed locations of these diffraction orders can be directly calculated using
26 the grating equation (Eq. 1).

27 **Supplementary Note 4. The cause of the banded pattern**

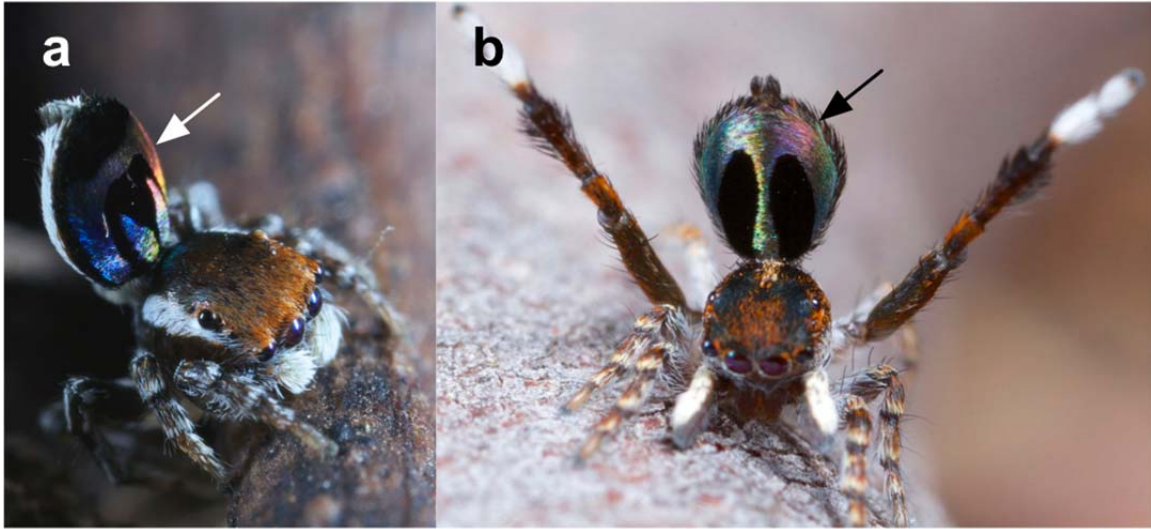
28 The banded diffraction profile is produced by the interaction between two individual
29 mechanisms. First, the reverse-ordered diffraction pattern that results from vertical surface
30 nanogratings. Second, the regular ordered diffraction pattern (Supplementary Fig. 6) that
31 results from multiple microscale prism/foil-shaped structures (Fig. 4d) acting as large period

32 horizontal microgratings (Supplementary Fig. 6). This interference resulted from the fact that
33 these structures were fabricated side-by-side in parallel (Fig. 4f&g).

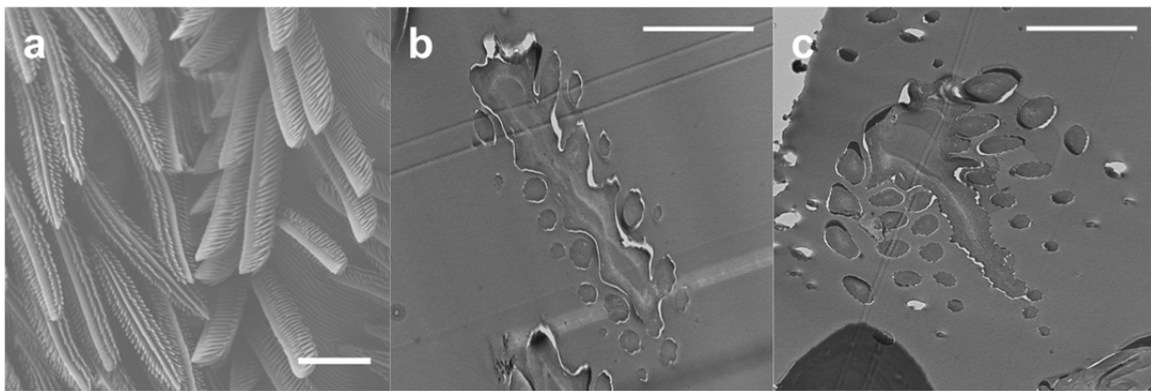
34 **Supplementary Note 5. Spider visual acuity**

35 *M. robinsoni* and *M. chrysomelas* are not likely to be able to discern the microscopic rainbow
36 patterns (Fig. 3a) resulting from individual scales because – Assuming the distance between a
37 male and a female during courtship is 1 cm (10,000 μm). We know from SEM/TEM micrographs
38 (Fig. 2) that the width of a single abdominal rainbow-iridescent scale is $\sim 10 \mu\text{m}$, which harbours
39 a double rainbow pattern, meaning each of the rainbow pattern spans $\sim 5 \mu\text{m}$ in width. For a *M.*
40 *robinsoni* or *M. chrysomelas* female to be able to resolve this rainbow pattern, she needs to
41 have a minimum acuity of α , where $\tan^{-1}(\alpha) = 5/10,000$. In other words, the female needs to
42 have an inter-receptor angle smaller than $1.7'$ to be capable of seeing the microscopic rainbow
43 patterns, which is beyond the smallest known inter-receptor angle ($2.4'$) in spiders (i.e., spiders
44 that have the highest acuity – *Portia* spp.)².

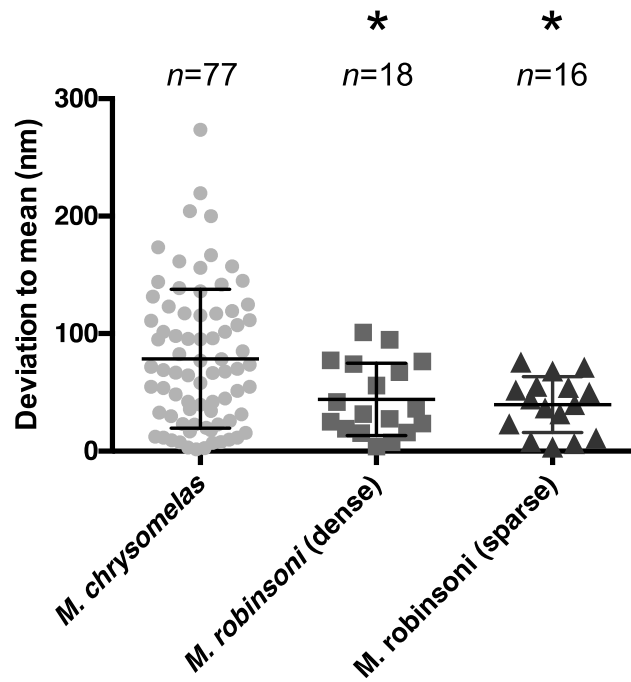
45



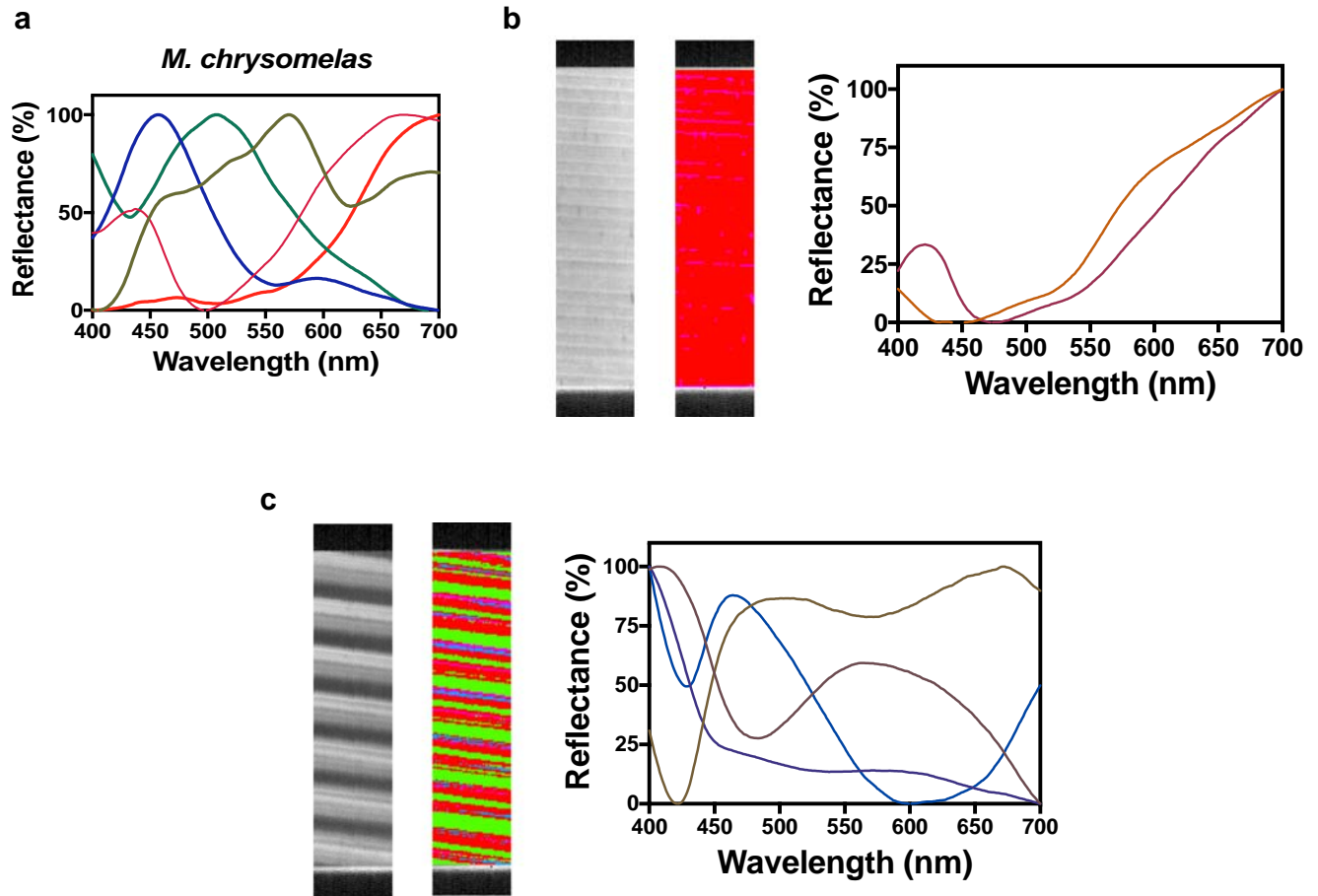
Supplementary Figure 1 | Images of *M. robinsoni* (a) and *M. chrysomelas* (b) engaged in their courtship dancing postures. Arrows show that they flatten and raise their abdomen to showcase the rainbow-iridescence to the potential mates.



Supplementary Figure 2 | Electron micrographs for the black scales of *M. robinsoni*. **a**, A SEM micrograph showing randomly orientated brush-like abdominal black scales. Scale bar: 20 μm . **b&c**, TEM micrographs showing the coronal (**b**) and transverse (**c**) views of a brush-like abdominal black scale. Granularly and heterogeneously deposited eumelanin is observed inside the black scale. Scale bar: 5 μm



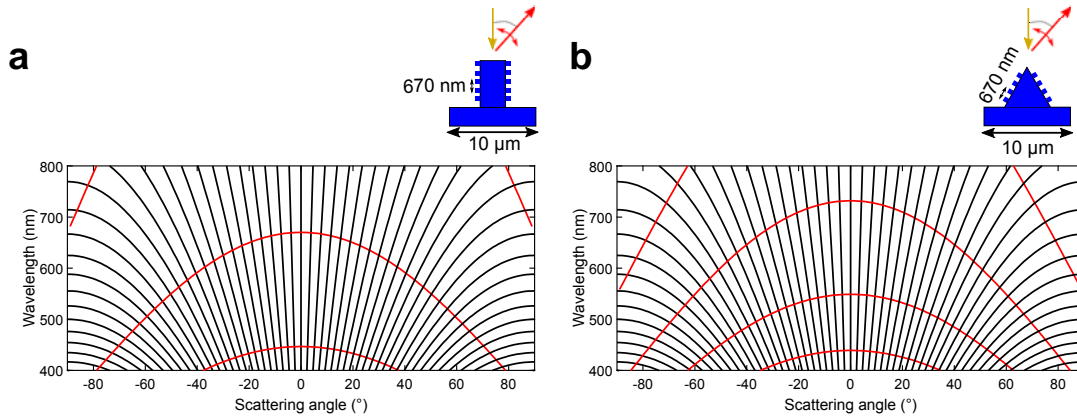
Supplementary Figure 3 | The grating period for the iridescent scales of *M. robinsoni* is more regular than that of *M. chrysomelas*. The distance of each individual spacing to the mean spacing ($D_{\text{individual}} - D_{\text{mean}}$) of the gratings are plotted (error bars: mean \pm s.d. Standard deviations are calculated based on all data points (n) of each data set.). The averaged “deviation to mean” values of *M. robinsoni* are significantly smaller (* represents $p \leq 0.05$) than that of *M. chrysomelas*, meaning the grating period is more regular in *M. robinsoni* than that in *M. chrysomelas*.



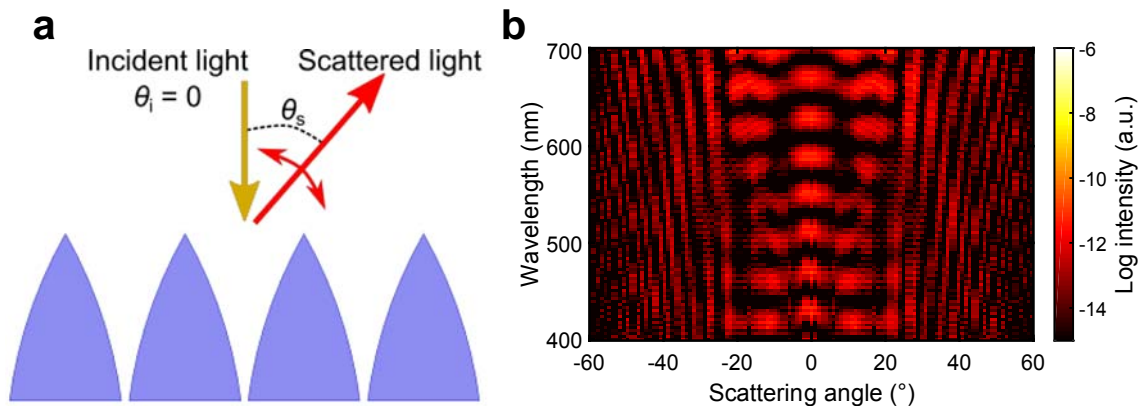
67

68 **Supplementary Figure 4 | Hyperspectral analysis results.** **a**, The reflectance spectra for the
 69 iridescent scales of *M. chrysomelas* collected by the hyperspectral imaging system show an
 70 array of rainbow colours. **b-c**, From left to right: the monochrome image, false-colour
 71 hyperspectral image, and the reflectance spectra collected by the hyperspectral imaging
 72 system from the flat (**b**) and prism (**c**) gratings. **b**, Shows predominantly monochromatic colour.
 73 **c**, Shows light diffraction with low resolving power. Hence, the prism grating produces the
 74 diffraction pattern with colours of low purity and saturation as seen in Fig. 6d inset. The colours
 75 of the reflectance spectra curves are estimated based on the “spec2rgb” function in R script
 76 “pavo”³. The colours in the false-colour hyperspectral images are arbitrarily assigned, each
 77 colour represents a different reflectance spectrum.

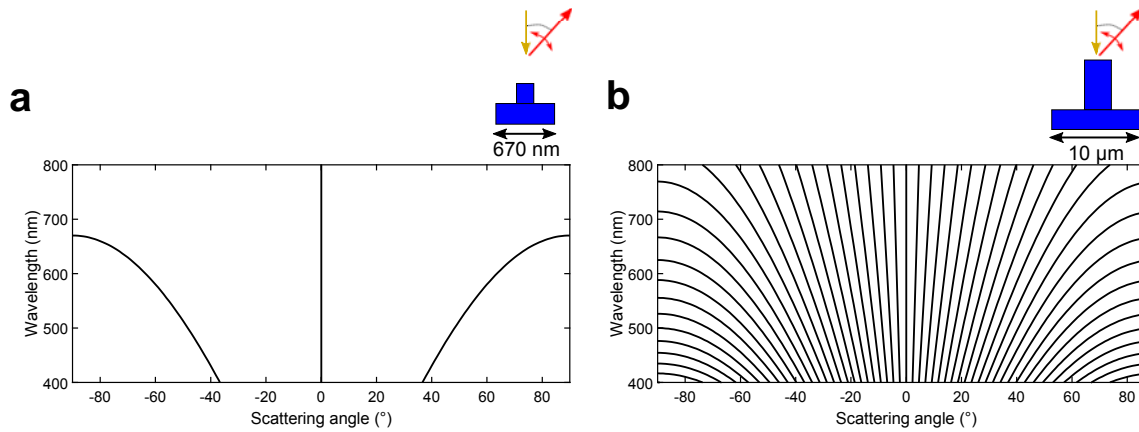
78



Supplementary Figure 5 | Analytical modelling of complex grating structures. a, Superposition of horizontal micro-grating (Eq. 1, black lines) and vertically aligned nano-grating (Eq. 2, red lines). **b,** Superposition of horizontal micro-grating (Eq. 1, black lines) and triangular (Eq. 3, red lines) nano-grating.



Supplementary Figure 6 | The simulated variable angle scattering spectra for the lenticular prism structures only. a, The simulation schematic for the microscopic lenticular prism structures without the surface nanogratings (Fig. 4d). **b,** The simulated result shows a normal diffraction pattern similar to that of the flat grating (Fig. 6g) with more allowed spectral orders (denser lines) due to the large period ($\sim 10 \mu\text{m}$).



Supplementary Figure 7 | Analytical modelling of horizontal grating structures. a, Horizontal nano-grating with 670 nm period. **b,** Horizontal micro-grating with 10 μm period.

Supplementary References

1. Palmer, C. & Loewen, E. DIFFRACTION GRATING HANDBOOK sixth edn. (Newport Corporation, 2005).
2. Land, M. F. in Neurobiology of Arachnids (Barth, F. G.) Ch. IV (Springer Berlin Heidelberg, 1985).
3. Maia, R., Eliason, C. M., Bitton, P.-P., Doucet, S. M. & Shawkey, M. D. pavo: an R package for the analysis, visualization and organization of spectral data. *Methods Ecol. Evol.* **4**, 906–913 (2013).